Journal of Solid State Chemistry 184 (2011) 2776–2784

Contents lists available at SciVerse ScienceDirect

Journal of Solid State Chemistry

journal homepage: www.elsevier.com/locate/jssc

# Oxygen stoichiometry control of nanometric oxide compounds: The case of titanium ferrites

N. Millot [a,*], P. Perriat [b]

[a] Laboratoire Interdisciplinaire Carnot de Bourgogne, U.M.R. 5209 C.N.R.S./Université de Bourgogne, BP 47 870, 21078 Dijon Cedex, France
[b] Matériaux, Ingénierie et Sciences, CNRS UMR 5510, INSA de Lyon, 69621 Villeurbanne Cedex, France

ARTICLE INFO

*Article history:*
Received 7 April 2011
Received in revised form
22 July 2011
Accepted 10 August 2011
Available online 16 August 2011

*Keywords:*
Oxygen stoichiometry
*In situ* X-ray diffraction
*In situ* conductivity
Nanometric particles
Ti-ferrites
Phase precipitation.

ABSTRACT

Three techniques have been coupled with an original device, based on $H_2/H_2O$ equilibrium, controlling oxygen partial pressure: XRD, TGA and DC conductivity in order to characterize very reactive compounds such as nanometric powders. From XRD, both the structure and the oxygen stoichiometry (thanks to their lattice parameter) were investigated *in situ*. From TGA, it was the oxygen stoichiometry (thanks to mass gain or loss) which was determined. From DC conductivity, it was both the structure and the oxygen stoichiometry (thanks to the activation energy) which were obtained. The advantages were to determine very rapidly and with a small amount of powder the equilibrium conditions ($T$, $pO_2$) necessary to obtain the desired phase and stoichiometry. These methods have been evaluated for nanometric titanium ferrites. Two phenomena have been observed during the reducing process: the precipitation of a rhombohedral phase and a significant grain growth linked together.



## 1. Introduction

The field of nanoparticles in materials research sparks intense interest due to their drastic size-dependent properties. In particular, these materials are very reactive with their outside environment due to high surface/volume ratio. For example, at the nanometric scale, to avoid the oxidation of metals, it is necessary to study them under reductive atmosphere [1,2]. Such constraints are also required for nanometric metal oxides containing unstable cations under ambient conditions (such as $Fe^{2+}$ [3]; $U^{4+}$ [4,5]; $Mn^{2+}$ [6]; $Cu^{2+}$ [7]). It is then necessary to develop synthesis routes under appropriate atmosphere (low $pO_2$, without water, etc.) coupled with *in situ* characterization tools.

"*Post mortem*" characterizations are usually used to determine both the structure and the oxygen stoichiometry of inorganic metallic oxides. Nevertheless, this methodology presents two major drawbacks. First, in order to obtain appropriate oxygen stoichiometry and structure, several time taking (usually days) thermal treatments and subsequent characterizations of a compound are necessary. Second, homogeneous samples are difficult to obtain. Indeed, as some cations (for example $Fe^{2+}$) are not thermodynamically stable in air, a significant amount of them can be oxidized when powders are studied under air atmosphere. This phenomenon leads to chemical heterogeneities in nanometric particles [8,9]. The purpose of this study was then to develop three *in situ* techniques: XRD, TGA and DC conductivity measurements to solve these problems and to determine precisely and rapidly the ($T$, $pO_2$) required for a desired nanomaterial

- From XRD experiments, it was both the structure and the oxygen stoichiometry (thanks to the lattice parameter) which can be investigated.
- From TGA measurements, it was the oxygen stoichiometry (thanks to mass gain or loss) which can be determined.
- From DC conductivity experiments, it was both the structure and the oxygen stoichiometry (thanks to the activation energy which was related to $M^{n+}/M^{n+1}$ cations pairs numbers) which could be investigated.

To valid these methods, ferrites, key materials in several important processes due to their magnetic and catalytic properties [10], in particular for biomedical applications [11], have been chosen, especially titanium ferrites $(Fe_{3-x}Ti_x)_{1-\delta}O_4$, with $x$ the Ti content in the spinel structure (between 0 and 1), and $\delta$ the deviation from oxygen stoichiometry. Very recently, titanium ferrites were used as magnetically separable sorbent for elemental mercury capture from the flue gas of coal-fired power plants [12]; it has also been shown that the introduction of Ti into magnetite structures has a remarkable effect on promoting the decolorization of synthetic dyes, proving that titanomagnetite

* Corresponding author. Fax: 33 3 80 39 61 67.
*E-mail address:* nmillot@u-bourgogne.fr (N. Millot).

0022-4596/$ - see front matter © 2011 Elsevier Inc. All rights reserved.
doi:10.1016/j.jssc.2011.08.007

could be useful for environmental remediation [13]. Titanomagnetites were also studied due to their paleomagnetic interest, since they were found in the earth crust as nanometer-scaled clusters [14,15]. Apart the evidence of a Verwey transition temperature shift in nanostructured Ti-ferrites [16], the choice of this material was also motivated by the fact that their cationic distribution has been extensively studied using several methods. Among the two types of sites occupied by the cations in the spinel structure [17], tetrahedral (A) or octahedral (B), the $Ti^{4+}$ cations reside only on the octahedral sites whatever the scale, micrometer [18,19] or nanometer-sized [20]. Only when the Fe cations are not completely oxidized, the location of the $Fe^{2+}$ cations is still subjected to controversial discussions [21,22].

## 2. Experimental procedure

Five compositions of titanium ferrites $(Fe_{3-x}Ti_x)_{1-\delta}O_4$ corresponding to: $x=0$, 0.25, 0.5, 0.75 and 1 have been synthesized according to a classical soft chemistry procedure. Such synthesis has already been reported elsewhere [23,24]. It is well known that the presence of divalent and trivalent cations is required in the formation of the spinel structure [25]. Briefly, after dissolution of suitable amounts of ferrous, ferric and titanium chloride (cations concentration 0.3 mol $L^{-1}$, pH < 1, $T=20$ °C) this mixture was added to an ammonia solution continuously stirred at 800 rpm at 20 °C, leading to instantaneous precipitation of nanometric particles. The equation of the reaction is the following:

$$(1+x)Fe^{2+}+(2-2x)Fe^{3+}+xTi^{4+}+8OH^{-}\rightarrow Fe_{3-x}Ti_xO_4+4H_2O \quad (1)$$

In accordance with the Ti and Fe solubility constants, the precipitate composition was the same as in the liquid phase (proven in Ref. [26] thanks to EDS, EELS, ICP and XPS analyses). The particles were then separated by centrifugation at 3500 rpm for 5 min and washed with deionized water under ultrasonification for 5 min followed by another centrifugation. After four successive washings, a sol was formed without surfactant nor dispersant addition. The sol was freeze-dried leading to a dry spinel precipitate. Calcination under optimized conditions was carried out to eliminate remaining impurities and to oxidize all the $Fe^{2+}$ cations while limiting crystallite growth. It consisted of a thermal treatment for 10 h under air at 380 °C for titanium amount $0.25 \le x \le 1$ and 330 °C for $x=0$ after a temperature ramp of 10 °C/h.

In order to reach the desired cation/oxygen ratio leading to $\delta=0$, powders were then annealed under $N_2/H_2/H_2O$ gas mixture [27]. Indeed, these gases were more appropriate than $CO/CO_2$ gas mixtures classically used at higher temperature (1000 °C). $H_2/H_2O$ mixtures ensured reducing atmosphere ($10^{-15} < pO_2 < 10^{-25}$ Pa) at the low temperatures required to limit grain growth (400–700 °C).

Each powder was studied by thermogravimetry using a symmetric thermobalance SETARAM TAG 24 capable of measuring weight variations of about 0.001%. The deviation from oxygen stoichiometry, $\delta$, was deduced from the mass changes observed during the oxidation and reduction treatments.

For infra-red spectroscopy (IR), nanoparticles (2 mg) were supported on 100 mg potassium bromide (KBr). Samples were mixed and ground using an agate morter and pestel. After grinding, samples were pressed into a disk of 13 mm diameter, using a pressure of 150 kg/$cm^3$. All spectra were recorded on a Perkin-Elmer 1725X FTIR spectrophotometer.

*In situ* X-ray diffraction (XRD) experiments were carried out using an INEL diffractometer equipped with a curved position-sensitive detector (CPS 120 INEL). Monochromatic Co-$K\alpha_1$ X-rays ($\lambda=0.17889$ nm) were obtained with a primary focusing Ge monochromator. The diffraction pattern was scanned over the $2\theta$ range 20–130° in steps of 0.03° and a counting time of 3600 s/step. *In situ* XRD experiments, using the XRK900 reaction chamber from Anton Parr, were carried out in the same oxido-reduction scheme as that performed in the thermobalance. *Ex situ* XRD patterns at room temperature were collected on a Siemens D5000 automatic powder diffractometer, operating at 35 mA and 50 kV. Fluorescence effects were minimized by using Cu $K\beta$ radiation and correction for instrumental broadening was determined from a standard reference material, annealed $BaF_2$. The lattice parameters of the powders were deduced from XRD line positions using a least-squares refinement method.[1] XRD line profile analysis[2] was performed in order to determine the average crystallite size (size of a region over which the diffraction is coherent) and the degree of crystallographic imperfections (microdistorsions, stacking faults, planar defects, etc.) [28,29].

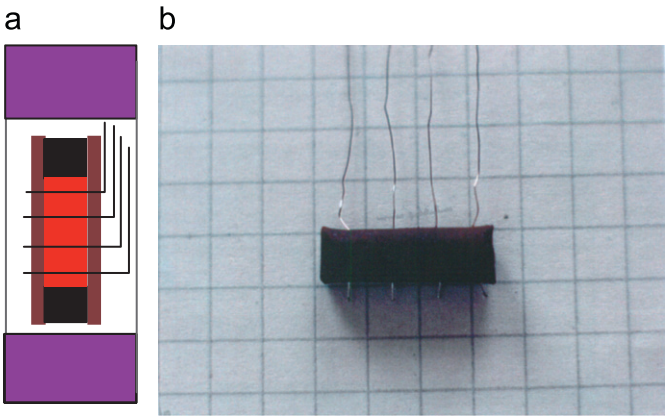


**Fig. 1.** (a) Scheme of the double encapsulation system developed in order to obtain cylindrical samples of nanopowders, with four platinum electrodes, by isostatic pressing. (b) Micrograph of such a cylindrical sample with four platinum electrodes used for DC conductivity measurements (scale: 5 mm × 5 mm).

The DC conductivity measurements were carried out under controlled atmosphere (air or reducing $N_2/H_2/H_2O$ mixtures) on compressed cylindrical samples using four-probe technique. The compact must satisfy the following compromises: to be sufficiently dense to have a good mechanical behavior but to be sufficiently porous to facilitate oxygen transport in its bulk. Also, by isostatic compaction under 250 MPa and thanks to a system of double encapsulation, cylindrical samples with four platinum electrodes were obtained (Fig. 1). Measurements were carried out with a Keitley 236 using the conventional four-probe technique. A current was applied through the outer probes inducing a voltage in the inner probes. Thus, the conductivity of the material was given by the formula $\sigma_{ferrite}=1/R_{ferrite}=I/U_{int}$.

Preparative furnace, in which DC conductivity measurements were realized, and TGA apparatus both contain an *in situ* $ZrO_2$ emf cell to measure $pO_2$.

Particle sizes were determined thanks to scanning electron microscopy (SEM) using a JEOL 6400F microscope.

Surface area measurements have been performed using an AUTOSORB apparatus and 150–200 mg of powder. Samples were outgassed *in situ* at 200 °C and the measurements were performed at liquid $N_2$ temperature with $N_2$ adsorbing gas. The generalized equation of BET has been used in calculation of surface area values from the isotherm of nitrogen adsorption. The mean

[1] In-house software taking into account the effect of sample gap.
[2] Available in the PC software package DIFFRACT AT supplied by SIEMENS.

apparent particle diameter was inferred from surface area, supposing that nanometric crystallites have a smooth and spherical shape with a narrow size distribution, using the equation $\emptyset_{BET}$ (nm)=6000/($\rho \times S$) where $S$ was the surface area ($m^2/g$) and $\rho$ the mass per volume unit calculated for the titanomagnetite, for example 5.06 $g/cm^3$ for $Fe_{2.5}Ti_{0.5}O_4$ (calculated thanks to the lattice parameter of Table 3).

## 3. Results and discussion

### 3.1. Research of the equilibrium conditions (T, $pO_2$) necessary to obtain in situ stoichiometric particles with the spinel structure, thanks to in situ X-ray diffraction

In order to obtain ($T$, $pO_2$) conditions leading to a stoichiometric material ($\delta=0$) crystallized with the spinel structure, X-ray Diffraction experiments have been carried out *in situ*. According to the literature concerning coarse grains ferrites submitted to a reducing treatment, the temperature range in which the spinel structure is obtained is very narrow and corresponds to a material close to the stoichiometric state $\delta \approx 0$ [15]. Thus, the XRD follow-up of phase transformation should permit to determine with precision the conditions for which the oxygen stoichiometry ($\delta \approx 0$) should be obtained. In addition, the comparison between the experimental cell parameter and that given in literature for $\delta=0$, may enable us to again define the conditions for obtaining a sample with $\delta \approx 0$ [14,21–22,30]. Indeed, the calculation of the cell parameter of the spinel phase during the reducing treatment, corrected by the thermal dilatation coefficient calculated for magnetite ($\alpha=1.25\times10^{-5}\,^{\circ}C^{-1}$), renders possible to stop the treatment precisely when the experimental cell parameter is close to that corresponding to stoichiometry. The XRD patterns obtained under reducing atmosphere, during a linear rise in temperature, are shown in Fig. 2. First, they allowed the description of a rhombohedral phase precipitation for the titanium compositions $x=0$, 0.75 and 1. The quantity of this phase was evaluated to be less than 10% and it was necessary to continue the treatment at higher temperature to make it disappear. The precipitation of the rhombohedral phase was always accompanied by an enlargement of the grains visible by the width reduction of the diffraction peaks (for instance the 311 reflection in Fig. 2) already highlighted and explained elsewhere by the exclusive presence of octahedral sites in this phase [26]. The temperatures necessary to obtain a pure spinel phase are gathered in Table 1. As expected, the measured cell parameter corresponded, for each composition, to the stoichiometric desired titanomagnetite $Fe_{3-x}Ti_xO_4$.

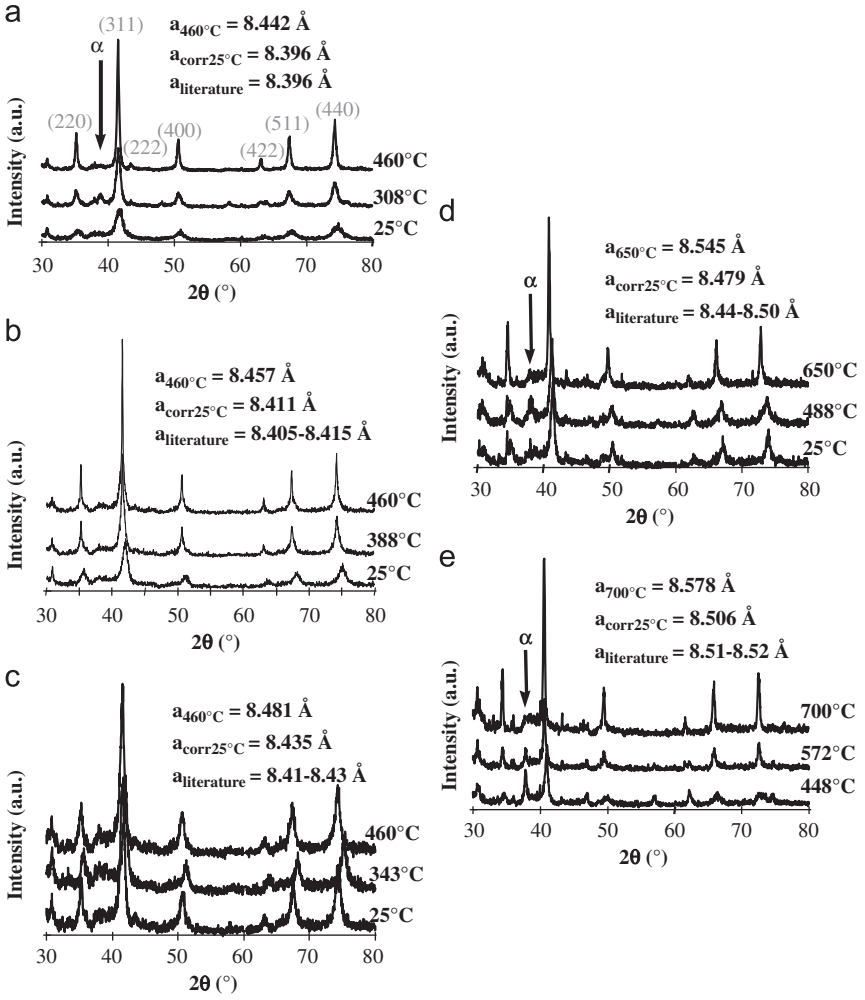


**Fig. 2.** XRD patterns of $(Fe_{3-x}Ti_x)_{1-\delta}O_4$ powders obtained *in situ* under $dN_2=0.15$ L $min^{-1}$ and $dH_2/H_2O=0.01$ L $min^{-1}$ during a temperature ramp of 2 °C $min^{-1}$ with a monochromatic $K\alpha_1$ Co radiation ($\lambda=0.17889$ nm): (a) $x=0$, (b) $x=0.25$, (c) $x=0.5$, (d) $x=0.75$, (e) $x=1$. The variations of the background level were due to the furnace. For the lattice parameters given in literature see references [14,21–22,30]. The experimental lattice parameter given at 25 °C has been corrected thanks to the dilatation coefficient of magnetite $\alpha=1.25\times10^{-5}\,^{\circ}C^{-1}$.

**Table 1**
Temperature and oxygen partial pressure determined thanks to TGA experiments and necessary to obtain the spinel phase with $\delta \approx 0$. Atmosphere: $dN_2 = 0.15$ L min$^{-1}$ and $dH_2/H_2O = 0.01$ L min$^{-1}$. $T_{start\ \alpha}$ was the temperature of appearance and $T_{end\ \alpha}$ that of disappearance of the rhombohedral phase. These temperatures were obtained by XRD analyses.

| | $Fe_{3-\delta}O_4$ | $(Fe_{2.75}Ti_{0.25})_{1-\delta}O_4$ | $(Fe_{2.5}Ti_{0.5})_{1-\delta}O_4$ | $(Fe_{2.25}Ti_{0.75})_{1-\delta}O_4$ | $(Fe_2Ti)_{1-\delta}O_4$ |
|---|---|---|---|---|---|
| $T_{red}$ (°C) | 460 | 460 | 460 | 650 | 700 |
| $pO_2$ (Pa) | $(3 \pm 1).10^{-26}$ | $(2 \pm 1).10^{-26}$ | $(8 \pm 1).10^{-27}$ | $(6 \pm 1).10^{-19}$ | $(1 \pm 1).10^{-17}$ |
| $T_{start\ \alpha}$ (°C) | 290 | – | – | 400 | 420 |
| $T_{end\ \alpha}$ (°C) | 320 | – | – | 590 | 680 |
| $\delta_{dynamic}$ | $-0.005 \pm 0.005$ | $-0.003 \pm 0.005$ | $-0.006 \pm 0.005$ | $0.022 \pm 0.005$ | $0.025 \pm 0.005$ |
| $\delta_{static}$ | $0.005 \pm 0.005$ | $0.008 \pm 0.005$ | $0.003 \pm 0.005$ | $0.020 \pm 0.005$ | $0.027 \pm 0.005$ |

$\delta$, deviation from oxygen stoichiometry of titanium ferrites $(Fe_{3-x}Ti_x)_{1-\delta}O_4$ was deduced from thermogravimetric analyses. $\delta_{dynamic}$ was determined *in situ* during the reducing treatment, thanks to mass loss during a linear ramp of 2 °C min$^{-1}$ (this value was corrected by subtraction of the loss due to both water and hydroxides adsorbed on cristallite surface). $\delta_{static}$ was obtained after the reducing treatment: 2 h at $T_{red}$. The gas flow was changed, first with $N_2$, then with $O_2$; $\delta_{static}$ was then determined thanks to the powder mass gain during the iron oxidation at this temperature.

### 3.2. Research of the equilibrium conditions (T, $pO_2$) necessary to obtain in situ stoichiometric particles with the spinel structure, thanks to thermogravimetric analysis

The particles obtained after the oxidizing heat treatment had size of about ten nanometers [26] and according to the broad absorption band around 1600 cm$^{-1}$ in their infra-red spectra, they possessed many $OH^-$ groups physically absorbed on their surface [31]. This is the reason why the mass loss due to the physically absorbed species (about 5%) was of the same order of magnitude as that due to the reduction of the $Fe^{3+}$ in $Fe^{2+}$ cations. Thus, a protocol allowing the separation of these two phenomena has been set up. The methodology employed consisted in systematically doubling all the thermogravimetric experiments by an experiment under the same conditions of temperature but under oxidizing conditions where only the water vapor loss was awaited. By difference of the two curves, it was then possible to make the share between the respective mass losses due to the adsorption of water and those due to the reduction of the $Fe^{3+}$ cations. Using this procedure, linear rises of temperature were carried out under $N_2/H_2/H_2O$ gas flows on titanium maghemite $(Fe_{3-x}Ti_x)_{1-\delta max}O_4$. The evolution of the oxidation state of powders was presented in Fig. 3. Only titanium compositions 0.25 and 0.5 show a one step reduction phenomenon. For the other compositions the differential curves presented several accidents due to the precipitation of the rhombohedral phase already highlighted by XRD. This precipitation slowed down the kinetics of reduction of the $Fe^{3+}$ cations in the case of the compositions $x = 0.75$ and 1. This is due to the higher valence of the cations in the rhombohedral phase than they had in the spinel structure ($Fe^{3+}$ instead of $Fe^{2+}$).

When $\delta$ was calculated during a linear rise of temperature, it was named $\delta_{dynamic}$. The evolution of $\delta_{dynamic}$ with temperature was shown in inset of Fig. 3. The lowest reduction temperature, $T_{red}$, allowing the synthesis of the spinel structure with $\delta \approx 0$ were gathered in Table 1. At these temperatures, the deviation from oxygen stoichiometry of the powders have been determined by applying other thermal conditions: after the linear rise of temperature under $N_2/H_2/H_2O$ mixtures until $T_{red}$, a two hours treatment was maintained under this atmosphere. After nitrogen purging, air was introduced in the TGA. From the mass gain then observed, $\delta_{static}$ was deduced and presented in Table 1. In all the cases, $\delta$ was close to 0, except for the large titanium contents samples for which a treatment at slightly higher temperature would have been desirable. However, a compromise between possible grain growth and deviation from oxygen stoichiometry (nearest to zero) was sought to avoid a significant enlargement of the grains.

### 3.3. Research of the equilibrium conditions (T, $pO_2$) necessary to obtain in situ stoichiometric particles with the spinel structure, thanks to conductivity measurements

The electrical conduction in ferrites is mainly due to electron hopping between ions of the same element, in the same sublattice (octahedral or tetrahedral sites) and with valence differing by one unit [32]. The activation energy of this phenomenon depends both on the concentration of the pairs responsible for conduction (for example $Fe^{2+}/Fe^{3+}$ pairs) and on the cation - cation distance: it is consequently the signature of the cationic distribution and of the crystalline structure of a product. Thus, by following-up the conductivity of the $(Fe_{3-x}Ti_x)_{1-\delta}O_4$ materials during the reducing treatment, the ($T$, $pO_2$) conditions necessary to obtain the stoichiometric spinel phase can be again determined.

The activation energy of the titanomaghemites $(Fe_{3-x}Ti_x)_{1-\delta max}O_4$ obtained after oxidizing heat treatment were calculated from the slope of the $\log \sigma = f(1/T)$ curves which were recorded under air atmosphere, in a linear decrease of temperature, and shown in gray in Fig. 4. For these powders, the composition is not modified when varying the temperature, the $Fe^{3+}$ cations being thermodynamically stable. The conductivity increase corresponds then entirely to the thermal activation of the intrinsic semiconductivity of the titanomaghemites. The activation energies so obtained are gathered in Table 2. All are approximately equal to 0.40 eV regardless of the titanium content, $x$. These experimental values were similar to those given by Creer [33] and Casalot [34] which found 0.5 eV for titanomaghemites rich in titanium and other substituted magnetites where any electronic exchanges between cations were also impossible.

The method employed to synthesize material with $\delta = 0$ was similar to that carried out by XRD. The conductivity that was recorded during a linear rise of temperature under reducing atmosphere is presented in black in Fig. 4. At the beginning of the experiment, the material was characterized by a maximal state of oxidation: $\delta = \delta_{max}$. The heating was then maintained until the slope of the $\log \sigma = f(1/T)$ curves coincided with the literatures values of activation energies characteristic of stoichiometry, i.e. 0.01 eV in the case of magnetite and 0.1 eV for other titanium compositions [35]. Activation energies were gathered in Table 2. For $x \neq 0$, they are independent of the Ti content and are approximately equal to 0.07 eV.

The conductivity recordings during the linear rise of temperature are shown Fig. 4, they provide information about the reduction kinetics of titanium ferrites. The complete interpretation of these curves is certainly complex because many phenomena occurred simultaneously, in particular for the materials $x = 0.25$ and 0.5 which had the smallest grains (Fig. 6). The large

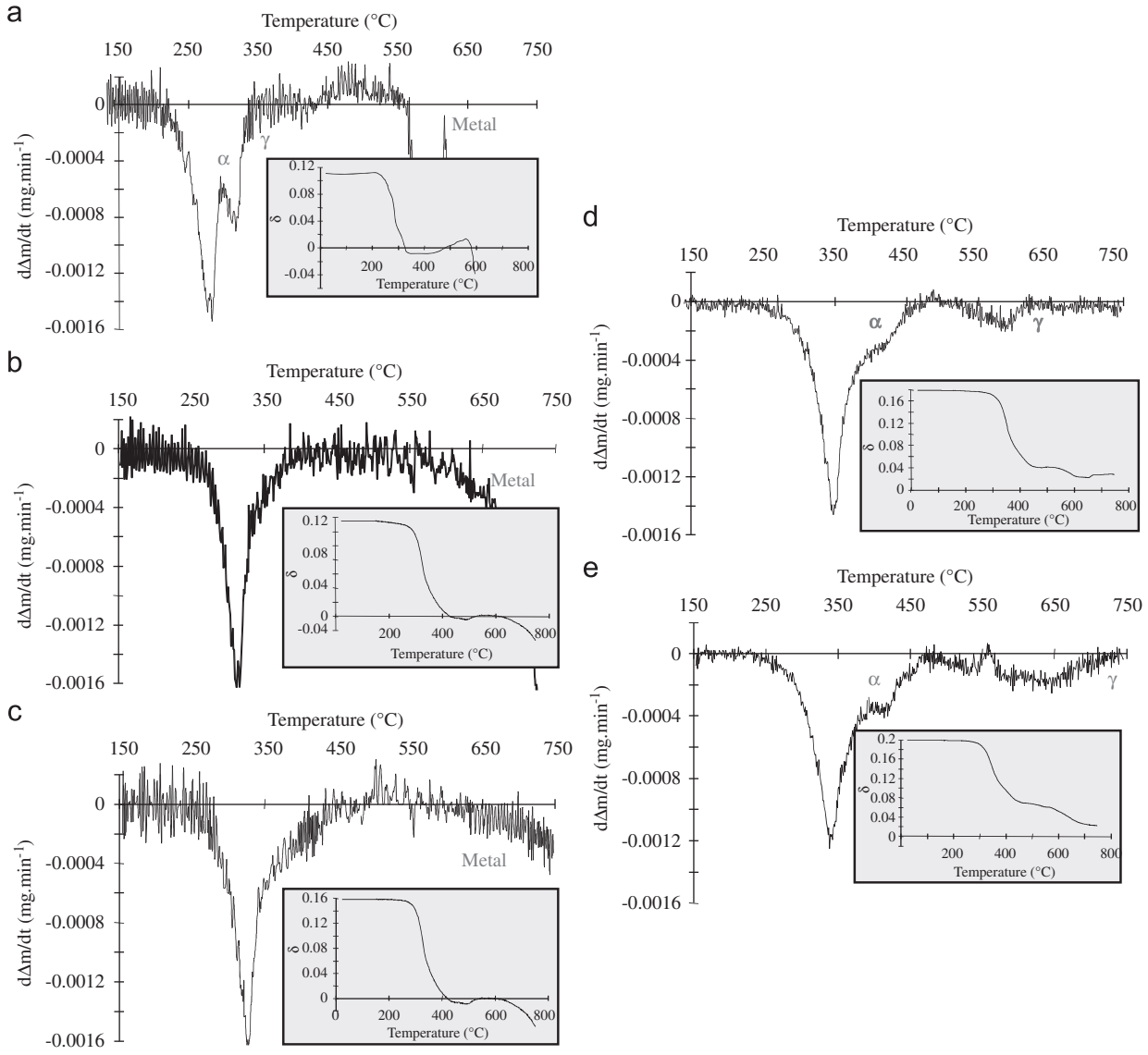


**Fig. 3.** DTG curves obtained during reduction treatment (linear temperature ramp of 2 °C $min^{-1}$ under $dN_2=0.15$ L $min^{-1}$ and $dH_2/H_2O=0.01$ L $min^{-1}$) of the $Fe_{3-x}Ti_xO_4$ compounds: (a) $x=0$, (b) $x=0.25$, (c) $x=0.5$; (d) $x=0.75$, (e) $x=1$. In inset, the deviation from oxygen stoichiometry $\delta_{dynamic}$ was represented as a function of temperature. $\alpha$ and $\gamma$ indicate the appearance and disappearance of the rhombohedral phase.

amount of water adsorbed on the surface of these grains (due to high specific surface, see Table 3) lead to electrical bridges which generated a constant conductivity equal to $10^{-4}\ \Omega^{-1}$ (Fig. 4b and c). It was then necessary to reach 200 °C to desorb water and then record the intrinsic conductivity of the material. After this first step, the general shape of the curves can be explained: during the linear rise in temperature under $N_2/H_2/H_2O$ atmosphere, the $Fe^{2+}/Fe^{3+}$ pairs number increased and conductivity consequently too. In the case of the $x=0.75$ and 1 titanium compositions, the precipitation of a $\alpha$-phase (conventional notation for the rhombohedral structure) was enlightened during the reducing heat treatment by the sharp variation of the conductivity that was generated. However, the conductivity which was measured remained that of the $\gamma$ phase (conventional notation for the cubic structure) only since the small quantity of the rhombohedral phase that precipitated (lower than 10% according to XRD patterns in Fig. 2) made any percolation impossible. The $\alpha$-phase precipitation was thus easily detectable by the conductivity jump induced in the $\gamma$ phase as one can see in Fig. 4d and e (this phenomenon was used as a principle for an oxygen sensor developed by Nakatani [36]). Indeed, for $x=0.75$ and 1 compositions, the conductivity decrease in the $\log(\sigma)=f(1/T)$ curve can be explained by the reduced number of $Fe^{2+}/Fe^{3+}$ pairs available in the $\gamma$ phase. It was then necessary to await the retransformation of $\alpha$ in $\gamma$ to observe again some conductivity increase. This phenomenon indicated that a significant proportion of the $Fe^{3+}$ cations initially present in the spinel phase were transferred into the rhombohedral phase during the precipitation of this latter. This implies that the titanium composition of the rhombohedral phase is less rich in titanium than in the well-known $FeTiO_3$ compounds (this latter composition containing only $Fe^{2+}$ should not consume any $Fe^{3+}$ cations of the spinel phase).

### 3.4. Characterization of the stoichiometric titanomagnetites obtained for various titanium rates

Thanks to the results of previous paragraphs, a series of stoichiometric titanomagnetites $Fe_{3-x}Ti_xO_4$ with different titanium contents have been synthesized ($\delta=0$). The temperature

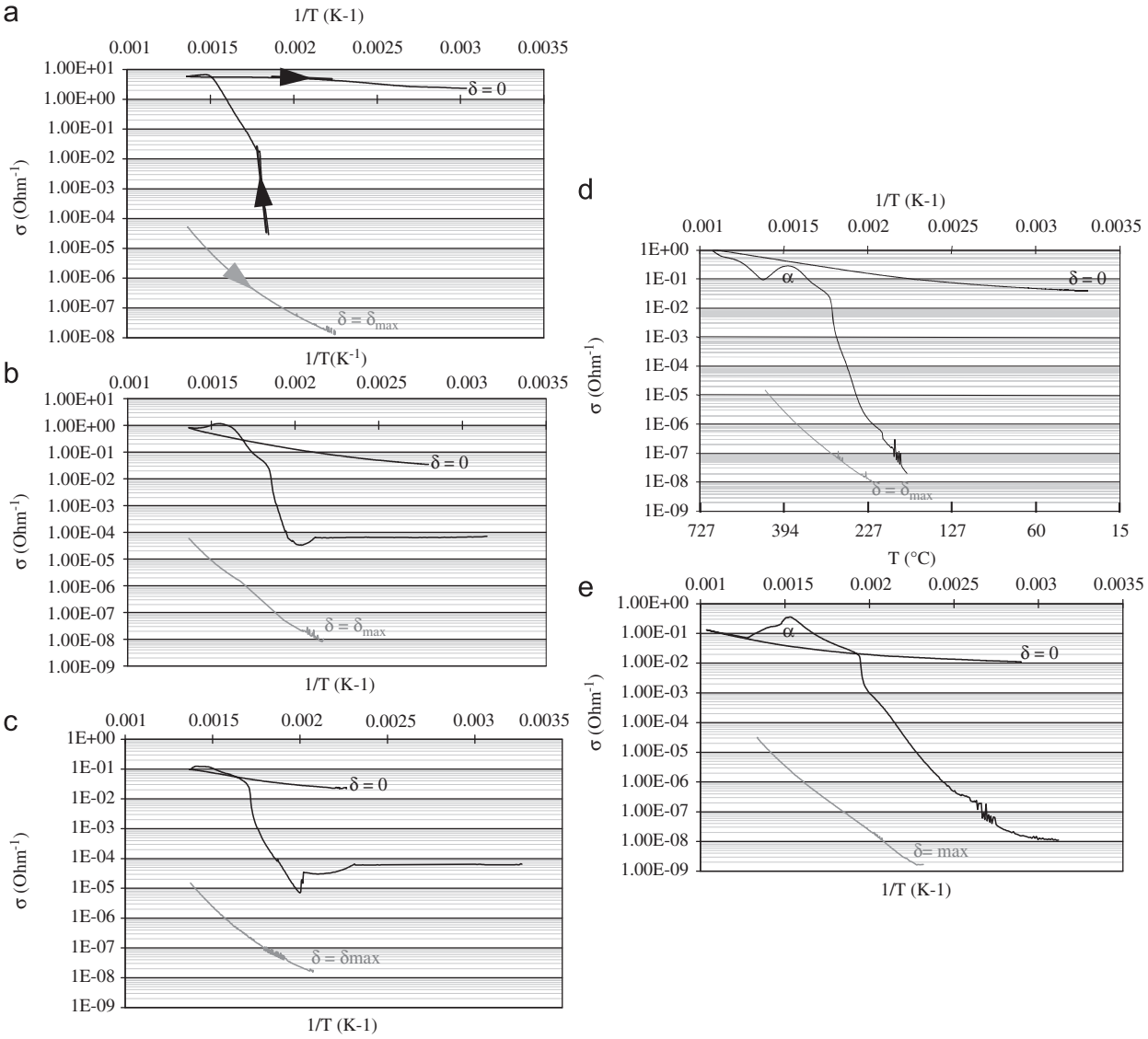


**Fig. 4.** In gray, the conductivity of $(Fe_{3-x}Ti_x)_{1-\delta max}O_4$ compounds during a linear temperature cooling (2 °C min$^{-1}$) under air atmosphere. In black, the conductivity of the $(Fe_{3-x}Ti_x)O_4$ compounds during a linear temperature cooling (2 °C min$^{-1}$) under $dN_2$=0.15 L min$^{-1}$ and $dH_2/H_2O$=0.01 L min$^{-1}$: (a) $x$=0, (b) $x$=0.25, (c) $x$=0.5, (d) $x$=0.75, (e) $x$=1. $\alpha$ indicated the appearance of the rhombohedral phase.

**Table 2**
Activation energies of the reduced $Fe_{3-x}Ti_xO_4$ powders and of the $(Fe_{3-x}Ti_x)_{1-\delta max}O_4$ powders whose iron cations were totally oxidized in $Fe^{3+}$.

| | $Fe_3O_4$ | $Fe_{2.75}Ti_{0.25}O_4$ | $Fe_{2.5}Ti_{0.5}O_4$ | $Fe_{2.25}Ti_{0.75}O_4$ | $Fe_2TiO_4$ |
|---|---|---|---|---|---|
| **$Ea_{red}$ $\delta \approx 0$ (eV)** | 0.01 | 0.07 | 0.07 | 0.08 | 0.07 |
| **$Ea_{ox}$ $\delta = \delta_{max}$ (eV)** | 0.38 | 0.42 | 0.37 | 0.42 | 0.40 |

and oxygen pressure required to elaborate such materials are summarized in Table 1, knowing that a two hours treatment was applied regardless of the composition.

The diffraction patterns recorded *ex situ* and shown Fig. 5 allow the precise analysis of line profile broadening (the presence of a furnace in case of *in situ* measurements made difficult the precise determination of these parameters). The average crystallite sizes of each titanium ferrite were calculated thanks to the Halder and Wagner method after Rietveld refinements [29]. These values are gathered in Table 3 and compared to the sizes deduced from surface area measurements. In the case of the titanium compositions $x$=0.25 and 0.5, the grains sizes determined by specific surface measurement are identical to those determined by the line profile analysis of the XRD reflections and are unchanged compared to powder size before the reducing treatment [26]. For these compositions, absolutely no grain growth occurred during the reducing treatment.

Scanning Electronic Microscopy (SEM) observations of the $Fe_{3-x}Ti_xO_4$ titanomagnetites confirmed in Fig. 6 that the $Fe_{2.75}Ti_{0.25}O_4$ and $Fe_{2.5}Ti_{0.5}O_4$ compounds are the only samples with nanometer sized particles and a homogeneous size distribution. On the contrary, the $x$=0, 0.75 and 1 compounds have grains sizes of a hundred nanometers due to the intragranular sintering that has accompanied the phase transformation. These results were confirmed by both surface area measurements and XRD line profile analysis ( (Table 3).

Infra-red spectra of the samples are shown in Fig. 7. Although the complete interpretation of the spectra is difficult due to the presence of cations of different valences (II, III, IV) in the two types of sites of the spinel structure, the spectra obtained are indicative of a pure spinel phase by means of the absorption

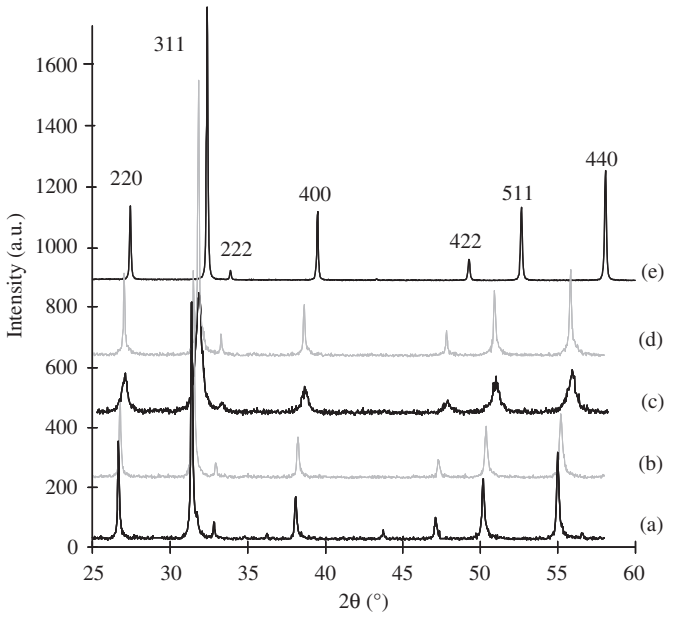


**Fig. 5.** X-ray diffraction patterns of $Fe_{3-x}Ti_xO_4$ powders obtained under air atmosphere and $K\beta$ Cu radiation ($\lambda$=0.154222 nm). All the peaks of the spinel phase were indexed.

bands $v_1$ and $v_2$ whose positions are given in Table 4. Moreover, these spectra are similar to those of titanomagnetites of neighbor compositions [37,38]. The creation of new vibration frequencies in the octahedral sites of the spinel structure, in particular Ti–O frequencies, lead to a widening of these bands for increasing titanium substitution. Moreover, a displacement towards high frequencies of the $v_2$ band was observed when $x$ increased (Table 4). This band can be attributed to the octahedral vibrations. During the iron substitution by titanium, the frequency of the $FeO_6$ group was gradually disturbed by the frequency of the $TiO_6$ group. This conclusion is in agreement with the theories of Waldron [39], White and DeAngelis [40] and with the experimental results of Gillot [37]. The small displacement of the $v_1$ band observed by B. Gillot is not visible in our spectra, perhaps because the substitution of $Fe^{3+}$ by $Fe^{2+}$ in tetrahedral sites did not disturb the vibrations frequencies of the $v_1$ band. Nevertheless, it should be noticed that the widening of the $v_1$ and $v_2$ bands made the precise bands positioning difficult. Absorption bands of weak intensity are also present in the spectra. A first one around 750 $cm^{-1}$ is characteristic of $Ti^{4+}$ cations: it is more and more marked and moves towards high frequencies when the titanium content increases, in agreement with previous observations in literature [30]. A second absorption band, characteristic of a direct spinel structure [41], appears around 310 $cm^{-1}$ in the spectrum of $Fe_2TiO_4$ ferrite (Fig. 7). It is consistent with the fact

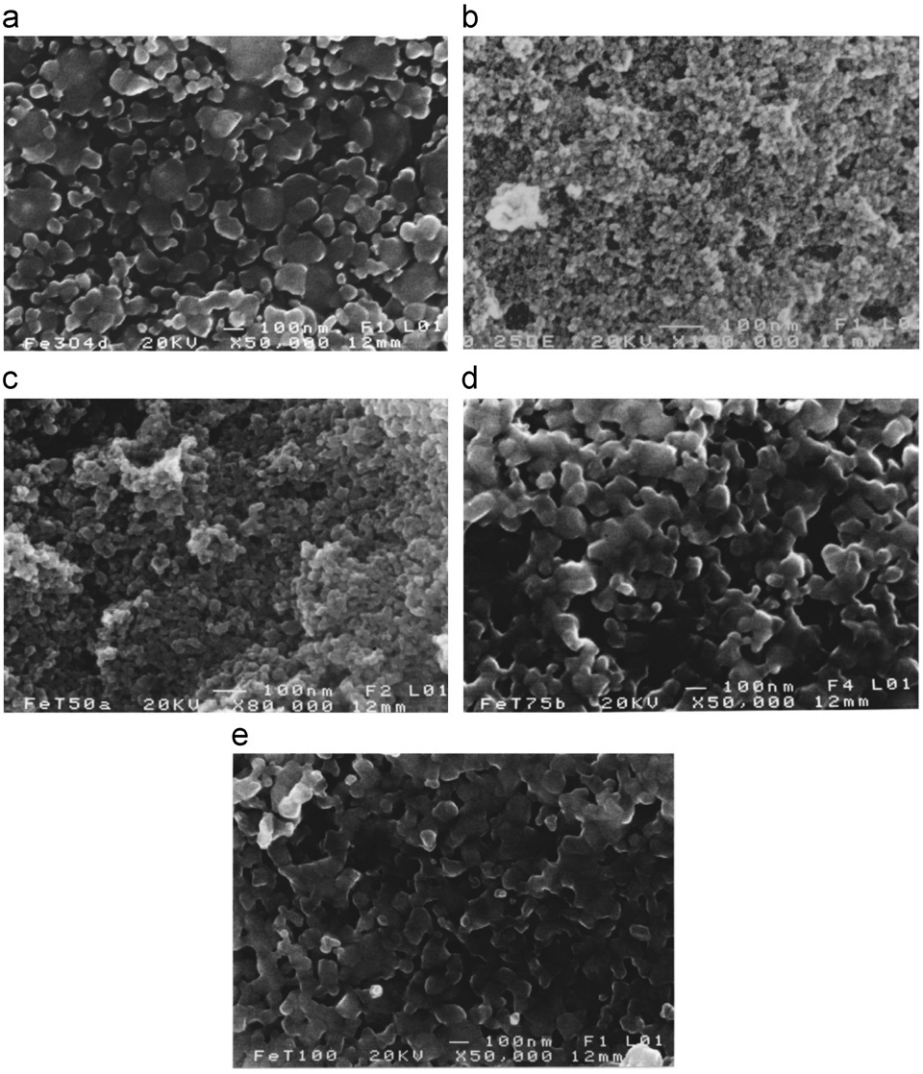


**Fig. 6.** Scanning Electron Micrograph of $Fe_{3-x}Ti_xO_4$ powders obtained after the reducing thermal treatment under $N_2/H_2/H_2O$ gas mixtures (a) $x$=0; (b) $x$=0.25; (c) $x$=0.5; (d) $x$=0.75; (e) $x$=1.

**Table 3**
Specific area measurements, particle size and lattice parameter of the $Fe_{3-x}Ti_xO_4$ powders. The particle size was deduced from X-ray diffraction analyses thanks to the Halder and Wagner method [29]. Lattice parameters were deduced *in situ* under controlled $pO_2$ atmosphere. Error in lattice parameter is over-estimated for the biggest particles in order to be comparable with those of the smallest.

| | $Fe_3O_4$ | $Fe_{2.75}Ti_{0.25}O_4$ | $Fe_{2.5}Ti_{0.5}O_4$ | $Fe_{2.25}Ti_{0.75}O_4$ | $Fe_2TiO_4$ |
|---|---|---|---|---|---|
| **S ($m^2$/g)** | $2 \pm 2$ | $81 \pm 2$ | $68 \pm 2$ | $7 \pm 2$ | $7 \pm 2$ |
| **$\emptyset_{BET}$ (nm)** | $600 \pm 300$ | $14.4 \pm 0.3$ | $17.5 \pm 0.3$ | $175 \pm 40$ | $180 \pm 40$ |
| **$\emptyset_{DRX}$ (nm)** | $100 \pm 5$ | $15 \pm 2$ | $18 \pm 2$ | $85 \pm 5$ | $105 \pm 5$ |
| **a (Å)** | $8.396 \pm 0.001$ | $8.408 \pm 0.001$ | $8.424 \pm 0.001$ | $8.493 \pm 0.001$ | $8.527 \pm 0.001$ |

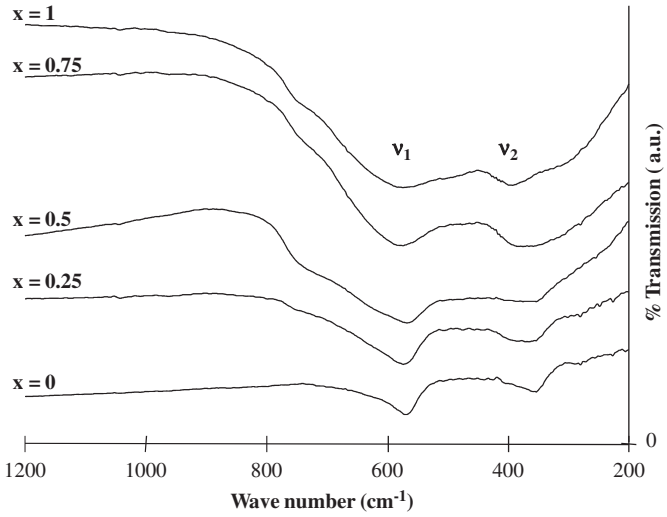


**Fig. 7.** Infra-red spectra in structure band area of the titanium ferrites $Fe_{3-x}Ti_xO_4$ obtained after reducing treatment under $N_2/H_2/H_2O$ gas mixtures.

**Table 4**
Positions of the IR absorption bands of the titanium ferrites $Fe_{3-x}Ti_xO_4$ obtained after the reducing treatment.

| | $x_{Ti}=0$ | $x_{Ti}=0.25$ | $x_{Ti}=0.5$ | $x_{Ti}=0.75$ | $x_{Ti}=1$ |
|---|---|---|---|---|---|
| $\nu_a$ | – | $745 \pm 2$ | $748 \pm 2$ | $755 \pm 2$ | $760 \pm 4$ |
| **$\nu_1$** | **$570 \pm 1$** | **$574 \pm 1$** | **$568 \pm 1$** | **$574 \pm 2$** | **$574 \pm 2$** |
| **$\nu_2$** | **$358 \pm 1$** | **$365 \pm 1$** | **$375 \pm 3$** | **$383 \pm 2$** | **$393 \pm 2$** |
| **$\nu_3$** | – | – | – | – | **$310 \pm 5$** |
| $\nu_b$ | $257 \pm 5$ | – | – | – | – |

that the tetrahedral sites of this compound contain only $Fe^{2+}$ while the average valence in the octahedral sites is three.

## 4. Conclusion

Thanks to *in situ* characterizations (thermogravimetry, XRD and conductivity), two phenomena have been observed during the reducing thermal processing of certain nanostructured titanium ferrites: the precipitation of a rhombohedral phase and a concomitant significant grain growth. The origin of these phenomena, which depend on the titanium ratio, has been explained by taking into account kinetics and thermodynamics considerations:

- For $x_{Ti} < 0.25$, the origin of the $\alpha$-precipitation was of kinetic nature. There was not enough titanium in the structure to stabilize the spinel phase and impede the $\gamma \rightarrow \alpha$ transformation observed in pure iron oxide. Indeed, $Ti^{4+}$ is significantly less mobile than $Fe^{2+}$ and $Fe^{3+}$ cations are and should severely limit both intergranular sintering and grain growth provided that it is in sufficient quantity. Thus, diffusion processes for low titanium contents are not sufficiently limited leading then to a $\gamma \rightarrow \alpha$ phase transition responsible for crystalline growth (the surface energy of the $\alpha$ phase being lower than that of the $\gamma$ one) [42].
- For $x_{Ti} > 0.5$, the origin of the $\alpha$-precipitation is rather thermodynamic. Indeed, if one refers to the phase equilibrium diagram of the Fe–Ti–O system existing for coarse grains [43], one can note the coexistence of a rhombohedral phase and of a spinel phase for large titanium contents in the temperature range explored in this paper. It is consequently necessary to treat the powder at higher temperature to obtain a pure spinel phase.

Finally, the $x=0.5$ titanium composition gives the best compromise between thermodynamic and kinetic constraints and renders possible the stabilization of the spinel phase with particle sizes of about 15 nm on all the range of its deviation from oxygen stoichiometry: $0 \leq \delta \leq \delta_{max}$.

More practically, the development of *in situ* investigations such as XRD, TGA and DC conductivity measurements, opens the door to fast and precise studies concerning the evolution of nanometric materials during different processes such as thermal treatments.

## Acknowledgment

This work is dedicated to Prof. Dr. Bolin Cheng (Academy of Sciences of Beijing), 1962–2006 who greatly contributed to this work.

## References

[1] Y. Champion, F. Bernard, N. Guigue-Millot, P. Perriat, Mater. Sci. Eng. A 360 (2003) 258.
[2] Y. Champion, F. Bernard, N. Millot, P. Perriat, Appl. Phys. Lett. 86 (2005) 231914.
[3] N. Millot, S. Bégin-Colin, P. Perriat, G. Le Caër, J. Solid State Chem. 139 (1998) 66.
[4] G. Rousseau, L. Desgranges, F. Charlot, N. Millot, J.C. Nièpce, M. Pijolat, F. Valdivieso, G. Baldinozzi, J.F. Bérar, J. Nucl. Mater. 355 (2006) 10–20.
[5] L. Quémard, L. Desgranges, V. Bouineau, M. Pijolat, G. Baldinozzi, N. Millot, J.C. Nièpce, A. Poulesquen, J. Eur. Ceram. Soc. 29 (2009) 2791.
[6] Y.F. Han, F. Chen, Z. Zhong, K. Ramesh, L. Chen, E. Widjaja, J. Phys. Chem. B 110 (2006) 24450.
[7] W. Yao, S. Yu, Y. Zhou, J. Jiang, Q. Wu, L. Zhang, J. Jiang, J. Phys. Chem. B 109 (2005) 14011.
[8] N. Guigue-Millot, Y. Champion, M.J. Hÿtch, F. Bernard, S. Bégin-Colin, P. Perriat, J. Phys. Chem. B 105 (29) (2001) 7125.
[9] B. Domenichini, P. Perriat, J. Merle, K. Basset, N. Guigue-Millot, S. Bourgeois, J. Mater. Chem. 9 (1999) 1179.
[10] D.L. Huber, Small 1 (2005) 482.
[11] B. Basly, D. Felder-Flesch, P. Perriat, S. Bégin, Chem. Commun. 46 (2010) 985.
[12] S. Yang, Y. Guo, N. Yan, D. Wu, H. He, Z. Qu, C. Yang, Q. Zhou, J. Jia, ACS Appl. Mater. Interfaces 3 (2011) 209.
[13] S. Yang, H. He, D. Wu, D. Chen, X. Liang, Z. Qin, M. Fan, J. Zhu, P. Yuan, Appl. Catal. B: Environ. 89 (2009) 527.
[14] W. O'Reilly, J. Magn. Magn. Mater. 137 (1994) 167.
[15] R. Dieckmann, H. Schmalzried, Ber. Bunseges. 81 (1977) 344.
[16] N. Guigue-Millot, N. Keller, P. Perriat, Phys. Rev. B 64 (2001) 012402.

[17] E.J. Verwey, E.L. Heilman, J. Chem. Phys. 15 (1947) 174.
[18] P.W. Readman, W. O'Reilly, J. Geomagn. Geoelectr. 24 (1972) 69.
[19] M. Ozima, M. Ozima, Phys. Earth Planet. Inter. 5 (1972) 87.
[20] J. Lorimier, F. Bernard, J.C. Niepce, N. Guigue-Millot, O. Isnard, J.F. Bérar, J. Appl. Cryst. 36 (2003) 301.
[21] L. Néel, Adv. Phys. 4 (1955) 191.
[22] R. Chevalier, J. Bolfa, S. Mathiew, Bull. Soc. Franc. Min. Crist. 78 (1955) 307.
[23] P. Perriat, E. Fries, N. Millot, B. Domenichini, Solid State Ionics 117 (1999) 175.
[24] N. Guigue-Millot, S. Bégin-Colin, Y. Champion, M.J. Hÿtch, G. Le Caër, P. Perriat, J. Solid State Chem. 170 (2003) 30.
[25] J.P. Jolivet, Metal Oxide Chemistry and Synthesis, John Wiley & sons, LTD 2000, Paris, 1994 (English translation of the original French text, De la Solution à l'Oxyde, InterEditions et CNRS Editions).
[26] N. Millot, D. Aymes, F. Bernard, J.C. Niepce, A. Traverse, F. Bourée, B.L. Cheng, P. Perriat, J. Phys. Chem. B 107 (2003) 5740.
[27] D. Aymes, N. Millot, V. Nivoix, P. Perriat, B. Gillot, Solid Sate Ionics 101–103 (1997) 261.
[28] J.I. Langford, National Institute of Standards and Technology, Special Publication, 846, 1992 (145 pp.).
[29] N.C. Halder, C.N.J. Wagner, Adv. X-ray Anal. 9 (1966) 91.
[30] B. Gillot, F. Jemmali, Mater. Chem. Phys. 15 (1986) 577.
[31] T. Belin, N. Millot, F. Villieras, O. Bertrand, J.P. Bellat, J. Phys. Chem. B 108 (17) (2004) 5333.
[32] E.J.W. Verwey, P.W. Haaijman, Physica 3 (1941) 979.
[33] K.M. Creer, J. Ibbetson, W. Drew, Geophys. J. 19 (1970) 93.
[34] A. Casalot, J. Claverie, P. Hagenmuller, J. Phys. Chem. Solids 34 (1973) 347.
[35] V.A.M. Brabers, Physica B 205 (1995) 143.
[36] Y. Nakatani, M. Matsuokka, Jpn. J. Appl. Phys. 22 (1983) 233.
[37] B. Gillot, Vib. Spectrosc. 6 (1994) 127.
[38] J. Bénard, A. Michel, J. Philibert, J. Talbot, Métallurgie Générale, Masson, Paris, 1989.
[39] R.D. Waldron, Phys. Rev. 99 (1955) 1727.
[40] W.B. White, B.A. DeAngelis, Spectrochim. Acta 23A (1967) 985.
[41] J. Preudhomme, P. Tarte, Spectrochim. Acta 27A (1971) 1817.
[42] P. Perriat, J.C. Niepce, G. Caboche, J. Therm. Anal. 41 (1994) 635.
[43] R.W. Taylor, J. Am. Ceram. Soc. 46 (1963) 278.